

Safe Trajectory Planning Using Reinforcement Learning for Self Driving

Josiah Coad¹, Zhiqian Qiao², John M. Dolan²

Abstract—Self-driving vehicles must be able to act intelligently in diverse and difficult environments, marked by high-dimensional state spaces, a myriad of optimization objectives and complex behaviors. Traditionally, classical optimization and search techniques have been applied to the problem of self-driving; but they do not fully address operations in environments with high-dimensional states and complex behaviors. Recently, imitation learning has been proposed for the task of self-driving; but it is labor-intensive to obtain enough training data. Reinforcement learning has been proposed as a way to directly control the car, but this has safety and comfort concerns. We propose using model-free reinforcement learning for the trajectory planning stage of self-driving and show that this approach allows us to operate the car in a more safe, general and comfortable manner, required for the task of self driving.

I. INTRODUCTION

Machine learning (ML) is an attractive approach to self driving, primarily because it is able to learn how to interact in a complex environment (too complex for rules) by minimizing a cost. Complexity comes from stochasticity, high-dimensional state spaces and/or intricate policies. Model-free reinforcement learning (RL) is a type of machine learning well-suited to self-driving, as it optimizes a policy which maximizes long-term rewards in a stochastic environment without the need for a model of the environment. Furthermore, RL does this without the need for laborious data collection, as in imitation learning. Furthermore, RL has been shown to outperform human experts on many games, so it could theoretically be better than human driver collected data (human error accounts for 90% of traffic accidents, so training our ML policies on such data may not be optimal.)

RL equipped with deep learning (DL) is able to learn complex policies in high-dimensional state spaces and continuous action spaces. However, in using any type of DL for the self-driving task, the question arises of whether a DL policy can respect the many self-driving constraints that should never get breached, such as colliding with a pedestrian or exceeding some maximum centripetal acceleration that would cause the car to flip. It is nontrivial to impose such constraints on a DL policy which is often a black box system.

Many current state-of-the-art RL self-driving approaches, such as [1], [2], [3], [4], [5] use control-based RL that outputs the next actuator control (steer, throttle) for the

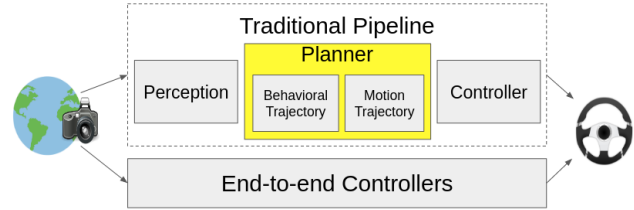


Fig. 1: A comparison of our method to end-to-end controllers. Hierarchical planners such as *Focused* and *Hierarchical* propose breaking planning into two parts. We propose using RL for generating the entire trajectory (shown in yellow).

vehicle. Most of these approaches train the policy end-to-end, meaning directly from camera input to car control output, thus bypassing the traditional pipeline of: perception, behavior choosing, motion planning, control. This has serious safety concerns since we have no idea how the DL model will steer and control the car until it generates the immediate next control.

Instead of bypassing the entire pipeline, we propose keeping the modules distinct and using RL to generate the behavioral trajectory (seen in green in Figure 3). We assume a separate perception module to extract the occupancy grid and speed limits. We then use a RL-trained policy to plan a trajectory given that information. We finally use feed the trajectory to a proportional integral derivative (PID) controller to generate the vehicle controls. By using trajectory planning instead of direct control, we can apply higher level safety systems to restrict the RL-generated trajectory if it is seen to take the car into an unsafe state, such as off the road or into an obstacle. See Figure 1 for a comparison of our method to the end-to-end control-based approach.

Our approach derives inspiration from several classical motion planning techniques, primarily *Focused* [6] and *Hierarchical* [7]. These hybrid approaches seek to combine two previously used techniques: low-fidelity grid search and path optimization. In the first step, they perform an exhaustive search over all possible discrete paths to choose an optimal behavioral trajectory. In the second, they perform a non-convex numerical path optimization to produce the final trajectory. However, the authors of these papers note a problem with breaking this up into two steps: we could be constraining ourselves to a local minimum by choosing a behavioral trajectory is only optimal in the discrete space. Thus, we find motivation to directly produce a smoothed out trajectory, which we can do with RL. Additionally, using RL is comparatively computationally cheap at test time since

¹Josiah Coad is with the Department of Computer Science & Engineering, Texas A&M University, College Station, TX, USA, josiahcoad@tamu.edu

²Zhiqian Qiao and John M. Dolan are with The Robotics Institute, Carnegie Mellon University, Pittsburgh, PA, USA, [zhiqianq, john}@andrew.cmu.edu](mailto:{zhiqianq, john}@andrew.cmu.edu)

it does not need to do an exhaustive search and numerical optimization at each step, but rather use a pretrained network to directly produce a trajectory.

In this paper, we propose a reinforcement learning based trajectory planner for self-driving. We show the advantage of this approach over both classical planning methods and reinforcement learning based controllers.

The structure of this paper is as follows: in Section II we present related works and how they motivate our approach. In Section III we formalize the problem and our solution. In Section IV we explain RL training details and our results. Finally, in Sections V and VI we summarize our contribution and provide directions for further work.

II. RELATED WORK

A. Non-machine Learning Trajectory Planning

Many non-deep learning approaches to trajectory planning have been proposed, roughly fitting into the categories of sampling, search and numerical optimization. Some examples of sampling planners are rapidly expanding random trees [8] and lattice sampling [6], [9], [10]. Many of these systems make strong simplifying assumptions about the environment, such as no uncertainty in an obstacle’s motions, or they severely discretize the planning space [11]. These systems also require extensive human engineering to tune. Thus, many of the traditional trajectory planners are not able to handle complex environments marked by a large state space, multifaceted objectives and many obstacles. Numerical optimization methods such as seen in [12], [13] also have been proposed for self-driving. In numerical optimization however, objects must be represented as differential mathematical functions, preferable convex, even though many states in the self-driving environment are discrete. This makes it difficult under the numerical optimization approach to consider all the objects that exist in a dense urban environment.

Our approach derives inspiration from several non-ML-based hierarchical methods. A hierarchical approach to trajectory planning was first proposed in *Focused* [6]. The two-step hierarchy starts with generating a low-fidelity spatiotemporal path through a node-layer network superimposed on the road. The authors use exhaustive search over all possible discrete paths to choose an optimal path through the road network. In the second step of this approach, the chosen path is fine-tuned. *Focused* was tested in single lane roads with sparse static obstacles.

Hierarchical [7] builds on *Focused* by also accounting for regulator elements such as stoplights and speed bumps. They first generate a low-fidelity path which they call a behavioral trajectory because the path and velocity profile chosen are greatly influenced by environmental factors such as obstacles, regulatory elements and road geometry and thus require behavioral choices. They then use this to create a fine-tuned trajectory called the motion trajectory.

In the past, behavioral choice has been implemented with finite state machines [14], [15], [16]. However, as *Hierarchical* points out, there are issues with this such as defining an interface between the behavior choice and the

trajectory planner. Thus, they point out that subsuming the behavioral planning into the trajectory planning can result in a more streamlined approach. RL has been proposed for the behavioral module previously, so we now propose to use RL for the behavioral trajectory generation.

For a more comprehensive review of non-machine learning approaches to trajectory planning and their limitations, refer to the surveys [11], [17], [18].

B. Imitation Learning-Based Trajectory Planning

Currently, imitation learning is the predominant deep learning-based approach used for trajectory planning. A straightforward way taken by [19] and others is to train a neural network to take camera input and output a layer of size $2H$ where H is the size of the horizon. The output represents a trajectory path $\langle x_{t+1}, y_{t+1}, \dots, x_{t+H}, y_{t+H} \rangle$. The goal is to minimize the displacement d_{t+i} between the expert’s actual trajectory point (x_{t+i}, y_{t+i}) and the predicted point $(\hat{x}_{t+i}, \hat{y}_{t+i})$:

$$d_{t+i} = ((x_{t+i} - \hat{x}_{t+i})^2 + (y_{t+i} - \hat{y}_{t+i})^2)^{\frac{1}{2}}$$

The loss is the mean squared error of the displacements. ChauffeurNet [20] does this with the addition of perturbations when collecting the trajectory samples for the sake of robustness.

In [21], the authors do something slightly different by aiming to learn the distribution parameters which maximize the likelihood of an expert path conditioned on the agent’s observation. They fit the imitative model in a supervised manner using a recurrent neural network. In a subsequent paper, NeuroTrajectory [22], the authors use imitation learning and evolutionary methods to learn to imitate expert drivers. Learning by Cheating [23] learned to extract a high-level state space and then used that to train an imitation learning-based planner.

Imitation learning still faces limitations, however, in that it requires large amounts of human driver training data, which is laborious to collect. Furthermore, the learned policy tends to overfit to the environment which it was trained on and could fail if presented with a vastly different situation, such as recovering from a near-crash scenario, if this scenario was not sufficiently covered in the training data. Thus, the trained algorithm may not react appropriately in these conditions in deployment. A recent paper argues that even with tens of millions of examples, direct imitation learning sometimes does not yield satisfactory driving policies [20].

C. End-to-End Reinforcement Learning Controllers

It is currently a common approach to use reinforcement learning to learn an end-to-end policy for directly controlling the car. In End-to-End Race Driving [1], the authors train an RL agent to drive a race car around a track by directly controlling the car with the agent. However, the ego vehicle exhibits aggressive unnecessary steering behavior and is not tested in any environment that includes other vehicles.

In [24], the authors use an RL agent to control the derivative of acceleration and steer, which is jerk and steering

rate. They claim this increases the comfort of the ride by reducing oscillatory and jerky behavior.

In the release of the CARLA simulator [5], the authors introduce a baseline end-to-end RL system that they used to compare in urban driving performance to a modular pipeline approach and an end-to-end IL approach. In their results, they found the end-to-end RL control approach to have inferior performance to the other approaches.

In the recent work [4], the authors note how difficult it is to get a good policy directly from a front camera. In response, they separately train the perception module to derive high-level features about the world and then train a control module, given the extracted world information. In CIRL [2] and [4] the authors introduce a gating unit which is used to choose which high-level behavior to follow (lane-following, left, right or straight) in urban driving. However, even in their best results, all these works still report crashes, motivating the need for future work.

Additional work in this area can be found in the surveys [25], [26]. The end-to-end control approach, while attractive for simplicity of implementation (the idea that one black box does it all), lacks interpretability and modularity, making it dubious for real world application in self-driving. Specifically, this approach is difficult to debug and to add higher-level logic to the system. Furthermore, control-based approaches have known problems of being jerky/oscillatory—see demo¹ from [1]. In addition, controls must be generated at a high and consistent frequency; and thus the system is brittle to any unexpected system latency. Finally, even in low-speed conditions when tested in simulators, these control-based approaches still suffer collisions, showing that more safety guarantees are needed before an RL-based solution can be used in industry.

Applying a safety constraint to a RL generated control, i.e. revoking the next steer or throttle if it is deemed that such an action would take the car into an unsafe state, would not work, since the car is often travelling at speeds that cannot be instantaneously stopped or diverted. Our approach of using RL for trajectory planning seeks to remedy these issues. Specifically, by planning a trajectory instead of directly controlling the car, we create a more interpretable and modular system and take advantage of that fact by applying a high-level safety constraint on the RL action to ensure safety of the action before execution.

III. METHODOLOGY

A. Trajectory Planning

The goal of trajectory planning is to find a sequence of states $\vec{q} = \langle q_1, q_2, \dots, q_n \rangle$ where $q_i = (x_i, y_i, speed_i)$ indicates the path that the ego vehicle should travel to avoid obstacles, respect road rules and maximize comfort and efficiency towards a goal. Once we obtain \vec{q} , we can pass it on to a controller, such as a PID controller. The PID outputs controls c to track the path where $c = (steering, throttle, brake)$ which is applied directly to the actuators of the car.

B. Reinforcement Learning

Reinforcement learning seeks to learn an optimal policy π parameterized by θ which maps a state (observation) s in the observation space \mathbb{S} to an action a in the action space \mathbb{A} , i.e. $\pi_\theta(a|s)$. In deep RL, θ are the weights to a neural network. Unlike supervised learning, RL does not require any labelled training data. Instead, RL interacts with an environment by being presented with s_t and choosing a_t according to its policy π . Under the assumption of full observability, RL operates on the premise that the environment can be viewed as a Markov decision process with a (possibly stochastic) transition function $T(s_{t+1}|s_t, a_t)$. The environment also returns a reward $R(s_t, a_t)$. The process of observing s_t , getting action a_t according to the policy π , and executing a_t in the environment is called a step. The reinforcement algorithm works to find the policy parameterization that maximizes the expected reward over the episode:

$$\operatorname{argmax}_\theta \mathbb{E}[R(s_t, a_t) | a_t \sim \pi_\theta(s_t), s_t \sim T(s_{t-1}, a_{t-1})] \quad (1)$$

Both continuous and discrete actions are possible with reinforcement learning, depending on the RL algorithm used. In the case of discrete, \mathbb{A} is a (generally small) finite action space. In the case of continuous, \mathbb{A} has a shape of $[-1, 1]^n$ where n is the number of controls contained in one action. The constraint to $[-1, 1]$ is trivial since we can scale the action once inside the step function. However, empirically this constraint is better for convergence. In our case, $n = 2H$ where H is the number of layers we are planning out to and 2 because for each point we pick, we also pick an associated velocity.

We use a reinforcement learning algorithm called Proximal Policy Optimization (PPO) [27]. PPO is a variant of the actor critic family that also includes an entropy term in its loss function to encourage exploration and clips policy changes so that policies do not update too drastically. It should be noted that our approach is not limited to use with PPO.

C. Safety Constraint

Because we are planning seconds into the future, we can detect potential traffic violations, kinematic violations and collisions with obstacles far before they happen and account for them. Call the planning space that results in one of these undesirable outcomes $-C^{free}$. Being able to account for collisions and violations is an advantage over reactive control-based RL, in which we don't know what control the RL agent is going to choose next until it is too late.

We need to somehow constrain the RL-chosen action to free space during planning, notated as C^{free} , which considers the occupancy grid and maximum centripetal acceleration. To do this, we first generate an action/trajectory proposal from our RL policy, calling this a . We then take the ℓ^2 norm of the residuals from a projection of a to C^{free} space and call the element in C^{free} that minimizes the ℓ^2 norm of the residuals, u^* , as seen in Equation 2.

$$u^* := P_{C^{free}}(a) = \operatorname{argmin}_{u \in C^{free}} \|a - u\|_2^2 \quad (2)$$

¹<https://youtu.be/e9jk-1BWF1w>

If the greatest absolute distance between the proposed trajectory and the projection is within some tolerance τ (we use $\tau = 0.5$), we allow the proposed action as is, else we choose u^* . If the Safety Constraint determines that there is no safe space, it throws an exception that can be handled by an emergency stopping module. This procedure is formalized in Algorithm 1.

Algorithm 1 Constraining RL Action to Safe Space

```

function SAFETY-CONSTRAINT(proposed trajectory  $a$ )
  find  $C^{free}$ 
  if  $C^{free}$  is empty then
    THROW NoPathException
   $u^* \leftarrow P_{C^{free}}(a)$ 
  if  $\max |u^* - a| < \tau$  then
    return  $a$ 
  else
    return  $u^*$ 

```

Using Algorithm 1, we can offer a much stronger assurance than control-based RL that collisions and other violations will not be encountered during deployment.

By allowing some tolerance in the path, we are allowing the RL to potentially chose a better path than what was in the discretized options. Yet, by restraining the deviance of the path, we still make a strong case for safety within the limits of our perception.

D. Environment

Once we obtain a bird's-eye view of the scene, we can map the Cartesian coordinate system to a curvilinear space to aid in planning. To do this, we first fit a curve to the road. In this paper, we use a third degree polynomial; but other curves such as a spline can be used. Next, equidistant perpendiculars can be drawn to this curve that make up layers along the road. The distance between layers is a function of speed. See Figure 2 for a demonstration of the transformation to bird's-eye. Now we have the scene in Cartesian (real-world) coordinates as seen in Figure 3(a). The distance along this curve, zeroed at the ego vehicle, makes the s curvilinear axis. Distance along the perpendiculars makes our n axis, as seen in Figure 3(b). A point (x_i, y_i) can be mapped to (s_i, n_i) by using a closest-point method such as quadratic minimization [28]. A point (s_i, n_i) can be mapped to (x_i, y_i) by moving along the original curve s_i distance and then moving n_i distance along the perpendicular. Finally, we convert curvilinear to a cell coordinate system by simply dividing n by lane width and s by layer distance (L), as seen in Figure 3(c).

E. State Space

As outlined in the previous subsection, we obtain a cellular representation of the environment. Our state space \mathbb{S} includes the static occupancy grid/matrix $O \in \{0, 1\}^{H \times W}$ and the speed regulatory grid $S \in \mathbb{R}^{H \times W}$ of those cells. H is the cellular depth of our sensor range, i.e. how far we plan out to and W is the cellular width of the road. The static occupancy

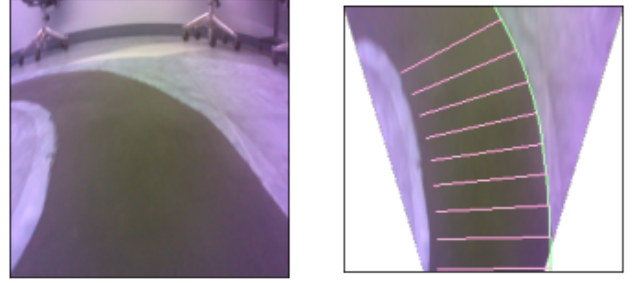


Fig. 2: Left is the view of the road from a front camera. Right is the result of the perception processing pipeline: transform to bird's-eye via a homography, run semantic segmentation to identify the road, fit third order polynomials to the road bounds and finally, derive normal lines to the edges to get the layers which we will plan along.

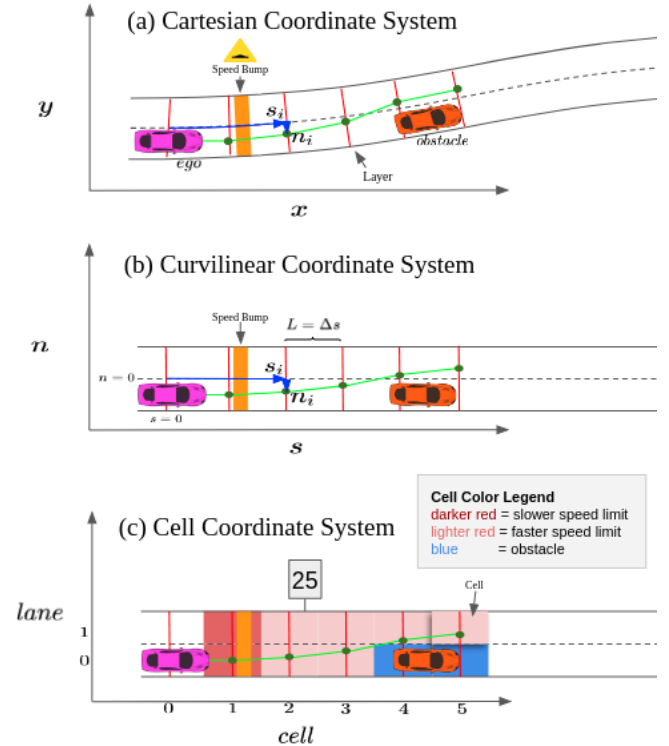


Fig. 3: Mapping a bird's-eye view (a) to a cell coordinate system (c) in which we plan. (s_i, n_i) shown in (a) gets mapped to the respective location in (b). Distance between layers is a function of speed and is denoted L . H is the sensor distance, i.e. how far we plan out to.

TABLE I: Reward Structure Terms

Cost Term	Name	Formula
f_i^r	speed error	$(v_i^{ref} - v_i)^2$
f_i^a	acceleration	$(v_i - v_{i-1})^2 / (2 \cdot dist_i)$
f_i^j	jerk	$f_{i+1}^a - f_i^a$
f_i^d	extra distance	$dist_i - L$
f_i^k	curvature	$(n_{i+1} - 2n_i + n_{i-2}) / L$
f_i^l	lane crossing	$\mathbb{1}[n_i, n_{i-1} \text{ in different lanes}]$
f_i^c	centripetal acceleration	$f_i^k \cdot v_i$

grid can be reasonably extracted from LIDAR. The speed regulatory grid can be extracted via an identification of regulatory elements (speed limit sign, stop sign, speed bump, etc.) using a camera, as was done in *Hierarchical*. Finally, the current lateral position n_0 and speed v_0 are included in the state space. In summary, $\mathbb{S} := \{O, S, n_0, v_0\}$. O and S can be rendered graphically as seen in Figure 3(c). Blue represents a 1 in O , i.e. the space is occupied. Shades of red represent entries in S with darker red representing slower speed limits.

Currently, \mathbb{S} is used as both a way to check if the proposed action is in C_{free} and as an input to our policy. However this is not a requirement; and indeed, it is an interesting direction for future work to feed a more complex state space to the policy, such as front camera footage, and only use \mathbb{S} for the subsequent safety constraint.

F. Action Space

The action space for the RL agent is of size $2H$ where H is the number of layers we are planning through, spaced out by some distance L between the layers in curvilinear space. The action space is defined as $a := \{[\Delta n | \Delta v] \in [-1, 1]^{2H}$ where Δp_j is the lateral change between layer $j-1$ and j and Δv_j is the velocity change between layer $j-1$ and j (where $j=0$ is defined as the current state). This action space can be converted to points n_j along each layer l_j by taking the cumulative sum, i.e. $n_j = \sum_{i=0}^j \Delta p_i$. Similarly, the same can be done for each respective v_j at each n_j .

G. Reward Structure

The reward function is made of a trajectory cost f which is a linear combination of chosen weights and the following terms: $f^r, f^a, f^j, f^d, f^k, f^l, f^c$. Each term is calculated by summing the individual components along the trajectory, i.e. $f^* = \sum_{i=0}^H f_i^*$. The f terms are described in Table I. Additionally, a success is given a reward of 10, a failure is given a reward of -20 and each step is given a reward of 1.

IV. EXPERIMENTS

A. Training details

In Figure 4 we show some of the episode rewards during training from 2M steps. The training was run on a Tesla K80 GPU with 32 parallelized environments using the PPO RL algorithm and took about 4 hours of wall time in our custom environment.

Each training episode was initialized with static obstacles appearing uniformly randomly over each cell drawn from a

Training Episode Rewards

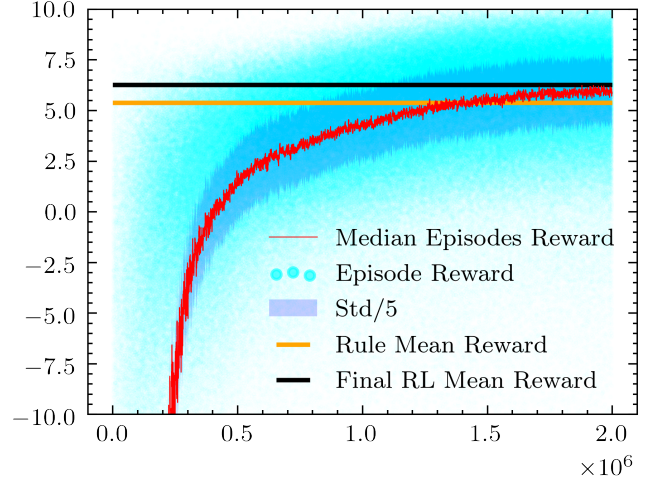


Fig. 4: Average episode rewards from two million steps of training for the RL trajectory planner. Red line is rolling window median with 1000 window length.

TABLE II: Hyperparameter settings for PPO

PPO Paper Name	SB PPO2 Name	Value
Number of actors	n_envs	32
Horizon (T)	n_steps	64
Minibatch size ¹	nminibatches	64
Discount (γ)	gamma	0.999
Adam stepsize	learning_rate	$2e^{-4}$
Entropy coefficient (c_2)	ent_coef	0.01
Clipping epsilon	cliprange	0.4
Number of epochs	noptepochs	25
GAE parameter (λ)	lam	0.99
Policy network	net_arch vf	FC: [64, 64]
Value network	net_arch pi	FC: [64, 64]

¹ nminibatches was set to 64 in the SB PPO2 implementation. However, this equals a minibatch size of 32 since $minibatch_size = (n_envs * n_steps) / nminibatches$.

Bernoulli ($p=0.5$) distribution. During training, we ensured that randomly generated obstacles did not fully block the road, until max-steps was reached. Once max-steps was reached, we blocked off the road with a wall. During training, the car planned 3 layers ahead, moved 3 layers and then replanned. During testing, the car planned 3 ahead and moved 1 layer before replanning.

B. Network Architecture

To represent the policy, we used a fully-connected (FC) multilayer perceptron network with two hidden layers of 64 units and tanh nonlinearities. The policy outputs the mean of a Gaussian distribution with variable standard deviations. We don't share parameters between the policy and value function (so coefficient c_1 from the original PPO paper is irrelevant.)

In Table II we outline the hyperparameter settings we found to work best. We used the Python package called Stable Baselines (SB) version 2.1 [29] for their implementation of Proximal Policy Optimization (PPO) called PPO2.

TABLE III: Driving Metrics from Figure 5

Measure	Aggregation	Exhaustive	RL (Ours)
Step Reward	mean	-1.49	-1.14
Acceleration	max	1.0	1.0
Jerk	max	1.4	0.3
Extra Distance	mean	0.3	0.1
Curvature	max	1.3	0.8
Centrip. Acc.	max	2.0	1.3

TABLE IV: Driving Metrics over 1000 Episodes

Measure	Aggregation	Exhaustive	RL (Ours)
Speed Track Err	Mean	7.582 ± 0.195	5.306 ± 0.126
Acceleration	Max	0.596 ± 0.017	0.367 ± 0.012
Jerk	Max	0.407 ± 0.012	0.194 ± 0.005
Excess Distance	Mean	0.317 ± 0.011	0.185 ± 0.007
Curvature	Max	0.738 ± 0.026	0.304 ± 0.010
Lane Changes	Sum	0.791 ± 0.027	0.960 ± 0.029
Centrip. Acc.	Max	1.367 ± 0.058	1.147 ± 0.036

C. Results

In Figure 5, we can see one of the advantages of using RL that plans in continuous search space. We compare to the discretized exhaustive search method and see that we obtain a smoother behavioral path with less drastic turns. This is also shown in Table III where we see that the RL results in a smoother and more efficient path.

Furthermore, using RL results in less latency to query for the next trajectory. One exhaustive search in the relatively small action space we used takes an average of $7.9e^{-3}$ seconds, while querying for the next trajectory from the RL policy takes $8.7e^{-4}$ seconds, making RL nearly a magnitude faster. This speed difference is crucial in real time computing requirements such as self-driving. Finally, we can see how the car comes to a safety stop before colliding with the wall as a result of the Safety Constraint from Algorithm 1. In static environments, assuming enough plan-ahead distance and proper perception, we can ensure 100% success rate, i.e. no collisions.

V. CONCLUSION

In this work, we are the first to our knowledge to propose using model-free reinforcement learning for the task of trajectory planning in self-driving. By using this approach, we garner the benefits of looking ahead by being able to apply safety constraints to our actions and we take advantage of the continuous action space of the RL agent. We show how our method has an advantage over control-based RL in that it results in less collisions and smoother rides. Furthermore, we show that it has an advantage over exhaustive discrete search-based methods in that it is computationally faster and results in smoother trajectories. The safety, interpretability, comfort and speed advantages of our system aim to make RL a viable option for future deployment in industry.

VI. FUTURE WORK

We are interested in extending this system to use inverse reinforcement learning to learn the reward function weights

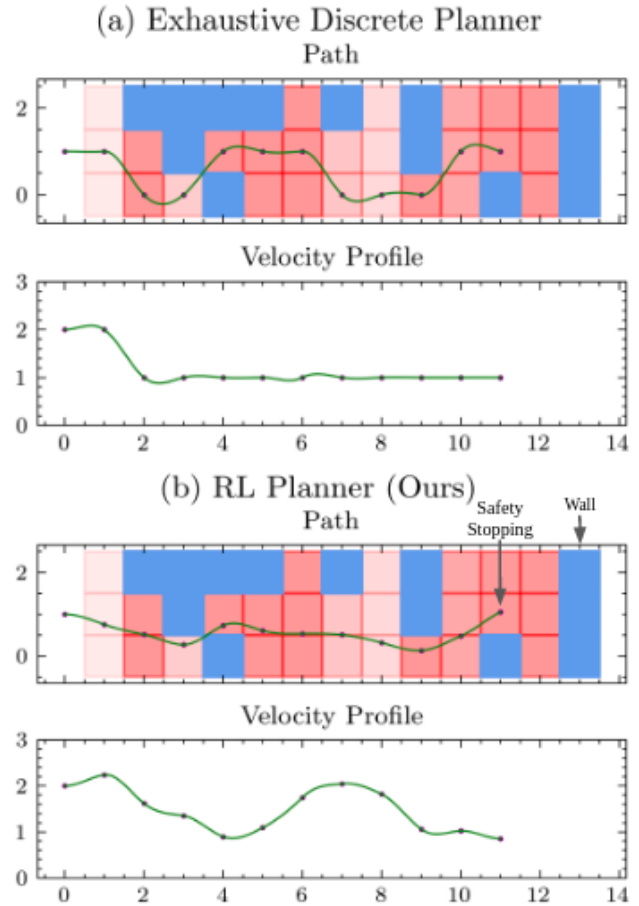


Fig. 5: In the Path figure, a three-lane road randomly populated with static obstacles and regulatory speeds is shown in cellular units. A wall appears at the end of the road. The purple dots represent points along each layer that the agent choose for the trajectory. In (a), the discrete exhaustive search chooses the optimal trajectory. In (b), we use RL to choose the optimal trajectory in a continuous action space along each layer. Green is a cubic spline which has been fit to the purple dots to form a path to travel along. In the Velocity Profile figure, the respective speeds chosen for each layer are shown. Numerical analysis of the paths are presented in Table III.

(instead of a human engineer picking all the tuning parameters as is now required). We also believe that incorporating an LSTM into our approach would allow capturing the partially observable (POMDP) nature of driving and would generalize our approach. We also wish to extend our approach to incorporate front camera data directly into our policy via a CNN, which would better take full advantage of the high capacity of our machine learning approach. We would also like to plan in dynamic environments and implement this system in a real world car.

VII. ACKNOWLEDGEMENTS

This material is based upon work supported by the National Science Foundation under Grant No. 1659774. We would like to thank the organizers of the Carnegie Mellon Robotics Institute Summer Scholars (RISS) program for making this experience possible.

REFERENCES

- [1] M. Jaritz, R. de Charette, M. Toromanoff, E. Perot, and F. Nashashibi, "End-to-end race driving with deep reinforcement learning," *CoRR*, vol. abs/1807.02371, 2018. [Online]. Available: <http://arxiv.org/abs/1807.02371>
- [2] X. Liang, T. Wang, L. Yang, and E. P. Xing, "CIRL: controllable imitative reinforcement learning for vision-based self-driving," *CoRR*, vol. abs/1807.03776, 2018. [Online]. Available: <http://arxiv.org/abs/1807.03776>
- [3] A. E. Sallab, M. Abdou, E. Perot, and S. Yogamani, "End-to-end deep reinforcement learning for lane keeping assist," 2016.
- [4] M. Toromanoff, E. Wirbel, and F. Moutarde, "End-to-end model-free reinforcement learning for urban driving using implicit affordances," 2019.
- [5] A. Dosovitskiy, G. Ros, F. Codevilla, A. López, and V. Koltun, "CARLA: an open urban driving simulator," *CoRR*, vol. abs/1711.03938, 2017. [Online]. Available: <http://arxiv.org/abs/1711.03938>
- [6] T. Gu, J. Snider, J. M. Dolan, and J. Lee, "Focused trajectory planning for autonomous on-road driving," in *2013 IEEE Intelligent Vehicles Symposium (IV)*, 2013, pp. 547–552.
- [7] W. Lim, S. Lee, M. Sunwoo, and K. Jo, "Hierarchical trajectory planning of an autonomous car based on the integration of a sampling and an optimization method," *IEEE Transactions on Intelligent Transportation Systems*, vol. 19, no. 2, pp. 613–626, 2018.
- [8] K. Macek, M. Becker, and R. Siegwart, "Motion planning for car-like vehicles in dynamic urban scenarios," in *2006 IEEE/RSJ International Conference on Intelligent Robots and Systems*, 2006, pp. 4375–4380.
- [9] K. Chu, M. Lee, and M. Sunwoo, "Local path planning for off-road autonomous driving with avoidance of static obstacles," *IEEE Transactions on Intelligent Transportation Systems*, vol. 13, no. 4, pp. 1599–1616, 2012.
- [10] J. Ziegler and C. Stiller, "Spatiotemporal state lattices for fast trajectory planning in dynamic on-road driving scenarios," in *2009 IEEE/RSJ International Conference on Intelligent Robots and Systems*, 2009, pp. 1879–1884.
- [11] W.-H. C. L. D. Christos Katrakazasa, Mohammed Quddusa, "Real-time motion planning methods for autonomous on-road driving: State-of-the-art and future research directions," *Transportation Research*, 2015.
- [12] J. Ziegler, P. Bender, M. Schreiber, H. Lategahn, T. Strauss, C. Stiller, T. Dang, U. Franke, N. Appenrodt, C. G. Keller, E. Kaus, R. G. Hertwich, C. Rabe, D. Pfeiffer, F. Lindner, F. Stein, F. Erbs, M. Enzweiler, C. Knöppel, J. Hipp, M. Haueis, M. Trepte, C. Brenk, A. Tamke, M. Ghanaat, M. Braun, A. Joos, H. Fritz, H. Mock, M. Hein, and E. Zeeb, "Making bertha drive—an autonomous journey on a historic route," *IEEE Intelligent Transportation Systems Magazine*, vol. 6, no. 2, pp. 8–20, 2014.
- [13] J. Ziegler, P. Bender, T. Dang, and C. Stiller, "Trajectory planning for bertha — a local, continuous method," in *2014 IEEE Intelligent Vehicles Symposium Proceedings*, 2014, pp. 450–457.
- [14] J. Kim, K. Jo, K. Chu, and M. Sunwoo, "Road-model-based and graph-structure-based hierarchical path-planning approach for autonomous vehicles," *Proceedings of the Institution of Mechanical Engineers, Part D: Journal of Automobile Engineering*, vol. 228, no. 8, pp. 909–928, 2014. [Online]. Available: <https://doi.org/10.1177/0954407014522443>
- [15] M. Montemerlo, J. Becker, S. Bhat, H. Dahlkamp, D. Dolgov, S. Ettinger, D. Haehnel, T. Hilden, G. Hoffmann, B. Huhnke *et al.*, "Junior: The stanford entry in the urban challenge," *Journal of field Robotics*, vol. 25, no. 9, pp. 569–597, 2008.
- [16] K. Jo, J. Kim, D. Kim, C. Jang, and M. Sunwoo, "Development of autonomous car – part ii: A case study on the implementation of an autonomous driving system based on distributed architecture," *IEEE Transactions on Industrial Electronics*, vol. 62, pp. 1–1, 08 2015.
- [17] B. Paden, M. Cáp, S. Z. Yong, D. S. Yershov, and E. Frazzoli, "A survey of motion planning and control techniques for self-driving urban vehicles," *CoRR*, vol. abs/1604.07446, 2016. [Online]. Available: <http://arxiv.org/abs/1604.07446>
- [18] D. González, J. Pérez, V. Milanés, and F. Nashashibi, "A review of motion planning techniques for automated vehicles," *IEEE Transactions on Intelligent Transportation Systems*, vol. 17, no. 4, pp. 1135–1145, 2016.
- [19] J. Chen, B. Yuan, and M. Tomizuka, "Deep imitation learning for autonomous driving in generic urban scenarios with enhanced safety," *CoRR*, vol. abs/1903.00640, 2019. [Online]. Available: <http://arxiv.org/abs/1903.00640>
- [20] M. Bansal, A. Krizhevsky, and A. S. Ogale, "Chauffeurnet: Learning to drive by imitating the best and synthesizing the worst," *CoRR*, vol. abs/1812.03079, 2018. [Online]. Available: <http://arxiv.org/abs/1812.03079>
- [21] N. Rhinehart, R. McAllister, and S. Levine, "Deep imitative models for flexible inference, planning, and control," *CoRR*, vol. abs/1810.06544, 2018. [Online]. Available: <http://arxiv.org/abs/1810.06544>
- [22] S. M. Grigorescu, B. Trasnea, L. Marina, A. Vasilcoi, and T. T. Cocias, "Neurotrajectory: A neuroevolutionary approach to local state trajectory learning for autonomous vehicles," *CoRR*, vol. abs/1906.10971, 2019. [Online]. Available: <http://arxiv.org/abs/1906.10971>
- [23] D. Chen, B. Zhou, V. Koltun, and P. Krähenbühl, "Learning by cheating," 2019.
- [24] D. M. Saxena, S. Bae, A. Nakhaei, K. Fujimura, and M. Likhachev, "Driving in dense traffic with model-free reinforcement learning," 2019.
- [25] S. Kuutti, R. Bowden, Y. Jin, P. Barber, and S. Fallah, "A survey of deep learning applications to autonomous vehicle control," 2019.
- [26] A. Tampuu, M. Semikin, N. Muhammad, D. Fishman, and T. Matiisen, "A survey of end-to-end driving: Architectures and training methods," 2020.
- [27] J. Schulman, F. Wolski, P. Dhariwal, A. Radford, and O. Klimov, "Proximal policy optimization algorithms," *CoRR*, vol. abs/1707.06347, 2017. [Online]. Available: <http://arxiv.org/abs/1707.06347>
- [28] H. Wang, J. Kearney, and K. Atkinson, "Robust and efficient computation of the closest point on a spline curve," 2002.
- [29] A. Hill, A. Raffin, M. Ernestus, A. Gleave, A. Kanervisto, R. Traore, P. Dhariwal, C. Hesse, O. Klimov, A. Nichol, M. Plappert, A. Radford, J. Schulman, S. Sidor, and Y. Wu, "Stable baselines," <https://github.com/hill-a/stable-baselines>, 2018.